



The Application of Autocorrelation SETI Search Techniques in an ATA Survey

G. R. Harp¹, R. F. Ackermann¹, Alfredo Astorga¹, Jack Arbutich¹, Jose Barrios¹, Kristin Hightower¹, Seth Meitzner¹, W. C. Barott², Michael C. Nolan³, D. G. Messerschmitt⁴, Douglas A. Vakoch¹, Seth Shostak¹, and J. C. Tarter¹

¹Center for SETI Research, SETI Institute, 189 Bernardo Ave., Ste. 100, Mountain View, CA 94043, USA

²Electrical & System Engineering Dept., Embry-Riddle Aeronautical University, 600 S. Clyde Morris Blvd., Daytona Beach, FL 32114, USA

³Arecibo Observatory, HC3 Box 53995, Arecibo, PR 00612, USA

⁴Department of Electrical Engineering and Computer Sciences, University of California at Berkeley, 387 Soda Hall, Berkeley, CA 94720-1776, USA

Received 2015 May 29; revised 2018 October 22; accepted 2018 October 22; published 2018 December 12

Abstract

We report a novel radio autocorrelation search for extraterrestrial intelligence. For selected frequencies across the terrestrial microwave window (1–10 GHz), observations were conducted at the Allen Telescope Array to identify artificial non-sinusoidal periodic signals with radio bandwidths greater than 4 Hz, which are capable of carrying substantial messages with symbol rates from 4 to 10^6 Hz. Out of 243 observations, about half (101) were directed toward sources with known continuum flux $> \sim 1$ Jy over the sampled bandwidth (quasars, pulsars, supernova remnants, and masers), based on the hypothesis that they might harbor heretofore undiscovered natural or artificial repetitive, phase or frequency modulation. The rest of the observations were directed mostly toward exoplanet stars with no previously discovered continuum flux. No signals attributable to extraterrestrial technology were found in this study. We conclude that the maximum probability that future observations like the ones described here will reveal repetitively modulated emissions is less than 5% for continuum sources and exoplanets alike. The paper concludes by describing a new approach to expanding this survey to many more targets and much greater sensitivity using archived data from interferometers all over the world.

Key words: astrobiology – instrumentation: detectors – instrumentation: interferometers – methods: data analysis – planetary systems – quasars: emission lines

1. Introduction

Searches for Extraterrestrial Intelligence (SETI) at radio frequencies traditionally focus on slowly modulated narrowband signals (Cocconi & Morrison 1959; Drake 1961; Oliver & Billingham 1971; Tarter 2001; Shuch 2011). The premise of the narrowband (~ 1 Hz) search is that relatively weak narrowband ETI signals may be present but hidden in ordinary astronomical observations.

An unspoken assumption is that all strong (> 1 Jy) radio sources already known to astronomers have a natural origin. This paper recognizes that this statement is not fully supported by existing observations. Some well-known strong radio sources might harbor a hidden message masquerading as, or piggybacking on, a strong natural source. While many pulsars and other sources may have been previously tested for repetitive power modulation, the authors are not aware of previous work testing for encodings that use, e.g., constant-power phase modulation from known bright sources. The latter is the focus here.

Suppose ET were to construct a powerful transmitter sending information at a bit rate between 10^3 and 10^9 Hz. To most radio telescopes, such a transmitter is indistinguishable from a natural continuum source because the time fluctuations are too short to appear in standard detectors. However, these same signals can be detectable by autocorrelating the electric field amplitude and phase, otherwise known as a field autocorrelation (FAC) detection. Here we present what we believe to be the first radio search for ETI using FAC detection of complex signals.

Recently, there has been a resurgence of theoretical research on searching for wideband engineered signals that may be used for interstellar messaging (Gardner & Spooner 1992; Harp et al. 2010a; Siemion et al. 2010; Messerschmitt 2012; Messerschmitt & Morrison 2012; Morrison 2012, 2017; Von Korff et al. 2013; Harp et al. 2015). Meanwhile, techniques developed for very long baseline interferometry have been adapted to capture

substantial bandwidths (> 1 MHz) of digitized time-series data for SETI postprocessing (Korpela et al. 2001; Harp et al. 2010a, 2015; Siemion et al. 2010; Tarter et al. 2010; Wayth et al. 2011; Morrison 2012). The benefit of archiving such data is that they may be processed in ways that could not be performed in real time. This paper reports SETI observations that make use of this nontraditional approach.

1.1. Conventional Matched Filter Bank Searches and AC

Searches for narrowband continuous and pulse signals depend upon the assumption of preconceived signal types. The prototypal ET signal appears as a narrow sloping or slightly curved trace in a frequency-versus-time plot or waterfall plot (see Figure 1). The intensity-inverted waterfalls of Figure 1 portray a narrowband signal from the *ISSE3* spacecraft (left) and a dispersed pulse of radiation from the Crab pulsar (right). To highlight the similarity of the waterfalls, the space and frequency axes are swapped between the left and right images. The *ISSE3* signal is not vertically aligned because of the relative acceleration between spacecraft and detector. The pulse is similarly slanted because light propagating in the cold plasma of the interstellar medium is dispersed (increasingly retarded at lower frequencies).

Searches for such signals look for modestly curved traces in the time-frequency domain having a small perpendicular cross-section (width \ll cross-width). Such searches can be parameterized with two to three independent parameters: the frequency f , slope or drift rate df/dt , and sometimes curvature or d^2f/dt^2 . In an equivalent pulse search, the time and frequency variables are swapped: t , dt/df , d^2t/df^2 .⁵

⁵ In practice, a fast search for naturally dispersed pulses can take advantage of the fact that the second and third parameters are codependent, thus requiring only a two-parameter MFB in the search (Zackay & Ofek 2017).

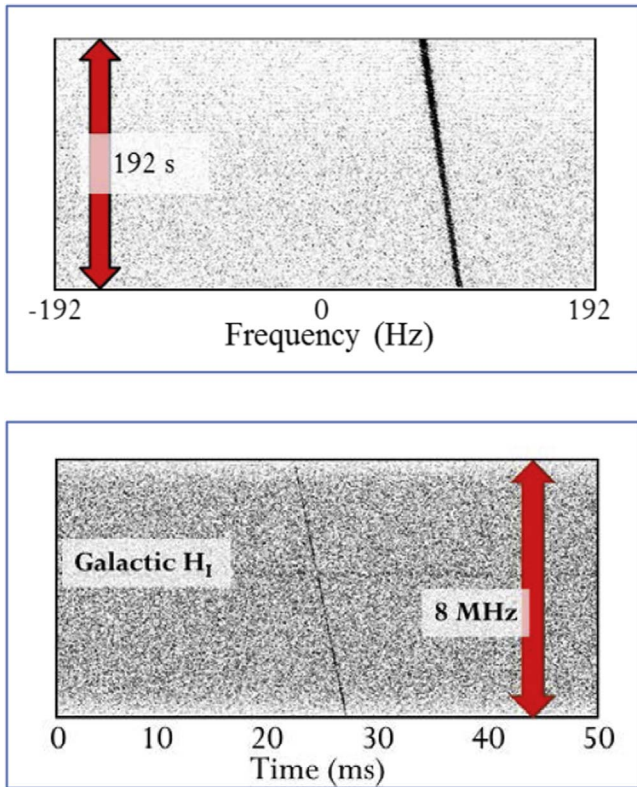


Figure 1. (Left) Time vs. frequency waterfalls taken at ATA, where the narrow dark trace indicates detection of a narrowband transmission from spacecraft *ISEE3* during its closest approach to Earth. (Right) Frequency vs. time waterfall, where the trace indicates detection of one wideband “giant pulse” from the Crab pulsar. The horizontal line in the Crab data corresponds to galactic H I emission at 1420 MHz.

Usually, signal searches use a matched filter bank (MFB), which effectively prepares a set of test waveforms spanning the parameter ranges and compares them to the observed waveform. The benefit of MFBs is their sensitivity. Historically, it has been argued that it is better to search a narrow parameter space with the greatest sensitivity than to search a wider parameter space with moderate sensitivity (Oliver & Billingham 1971).

In this campaign, we use AC detection rather than an MFB. The search philosophy is that AC searches for wide-bandwidth⁶ signals and can piggyback on MFB narrowband searches requiring only nominal extra processing. For weak signals, AC detection is less sensitive than narrowband detection for the same ET transmission power. Yet AC is sensitive to a different and larger class of signals that generally do not appear in narrowband searches. Thus, we broaden the possibilities for detection of an artificial signal with only a small additional computational expense. We argue that in future searches, it makes sense to implement both narrowband and AC detectors for a more effective search, especially when observing with radio interferometers.

1.2. Research Hypotheses

Because there is little previous work on FAC surveys, it is difficult to quantify the state of our knowledge at the beginning

of this survey. For definiteness, we introduce two simplistic hypotheses that encapsulate our goals (with more detail to be found in the analysis section).

Hypothesis 1. The emitted electric fields of many previously discovered strong radio sources with flux >1 Jy are modulated with a repeating pattern either directly by extraterrestrials or due to some heretofore unknown physics. **Hypothesis 2.** Many exoplanets emit moderate-bandwidth (e.g., 1 MHz) artificial signals that were not previously discoverable in continuum surveys or in narrowband ETI searches. If such signals contain repetitive structure, they can be detected by autocorrelation.

To the best of our knowledge, these hypotheses cannot be excluded based on past observations, and the results here represent a new foray into the SETI.

This survey focuses only on moderate-bandwidth repetitive signals with waveforms substantially more complex than pure sinusoids. The SETI Institute already has a sensitive ultra-high-resolution spectrometer used for narrowband searches, but instrumental limitations prevented the pursuit of a commensal narrowband search along with the AC search. Low-resolution power spectra were generated from all the data described here to verify data quality, but the frequency resolution of these power spectra was not good enough to pursue a narrowband search.

Besides the source types mentioned above, this campaign includes a small number of targets with special interest for SETI, such as the galactic anticenter and the Earth–Sun Lagrange L4 point, and many reference observations used as comparators for testing the direction of origin of candidate signals.

The rest of the paper is divided into six interconnected parts. Section 2 introduces the autocorrelation methods used here and provides a careful discussion of the cost/benefit analysis of autocorrelation as compared with more conventional matched-filter SETI searches (i.e., narrowband search). We show some of the advantages of autocorrelation (e.g., insensitive to dispersion in the interstellar medium, enhanced sensitivity to repetitive signals) and compare the relative sensitivities of common detectors for artificial signals. Section 3 outlines the observational parameters and summarizes the survey results, including a few examples of identified Earth-originating technological signals. Section 4 provides a discussion and interpretation of the survey results. Having established the utility of an autocorrelation detector, Section 4 demonstrates another method for autocorrelation detection that can be applied to widely available archive (correlator) data from radio interferometers all over the world. We outline how an archive survey might be undertaken and discuss other possible future directions for research.

Section 5 summarizes the main results and makes concluding statements. Finally, the Appendix provides the important details of the specific digital/numerical implementation of autocorrelation in this study. This is necessary because there are multiple digital implementations that could conceivably be called autocorrelation detectors.

2. Signal Detection Algorithms

Autocorrelation-based detection strategies are a useful addition to the tool kit of the traditional SETI narrowband search. Autocorrelation (1) is sensitive to a wide class of

⁶ What is considered wide-bandwidth is relative to the very narrow bandwidth signals of conventional searches. In this paper, AC signals with bandwidth up to 7 MHz are compared with typical 1 Hz bandwidth signals in conventional SETI.

signals that are not effectively detected in a narrowband search, (2) has the potential for detecting signals containing messages with substantial information rates,⁷ and (3) is insensitive to dispersion in the interstellar medium (Harp et al. 2010a), since identical signals subject to the same dispersion remain identical. The last point is crucial, since wideband radio signals are strongly dispersed in the interstellar medium, and this can otherwise obfuscate the detection.

We demonstrate their immunity to dispersion with a simulation. We model a distant transmitter emitting four short pulses of sinusoidal radiation at 1 GHz and emitted over a period of 4000 s as in Figure 2 (left; solid line). After traveling 1600 lt-yr through a plasma with a mean electron density equal to that of the galactic interstellar medium ($0.01 \text{ e}^- \text{ cm}^{-3}$), the dispersion measure (DM) of the signals will be about 5 pc cm^{-3} . Applying the well-known formula for cold plasma dispersion, an estimate of the DM is (Cordes 2002) delay (s) = $0.00415 \text{ DM}/f^2$ (GHz). We calculate the pulse (electric field) amplitudes as they would appear at the receiver (Figure 2, left; green dots). After dispersion, the pulses are broadened and have lower peak intensity. (During the time period near 2000 s, two of the dispersed pulses overlap and coherently interfere, but this has no impact on subsequent pulse reconstruction.) In the right panel of Figure 2, we display the complex-valued FAC (algorithm defined below) of the received signal with itself (lavender lines). As expected, the FAC detector shows six spikes for the original four pulses (a zero-delay spike has been suppressed). The FAC response is compared to another method, intensity autocorrelation (IAC; green dots).

The example of Figure 2 visualizes our general point: an FAC filter detects a coherent⁸ repetitive signal passed through any stationary linear filter just the same as if the data are not filtered. Hence, FAC is not only immune to dispersion but also resistant to the effects of slowly varying scintillation (time-scales longer than the observation period) in the interstellar medium.

The FAC discriminates between natural and engineered signals. For the engineered coherent pulses modeled in Figure 2, FAC discrimination (height of peaks compared to surrounding values) is generally quite good, provided the received signal has a sufficient signal-to-noise ratio (S/N; see below). By comparison, pulsars and quasars emit light that is not coherent over long periods of time or detected with FAC. This is why FAC is not used for pulsar searches. As far as we know, only artificial, engineered processes can give rise to signals detectable in FAC.

The coherent FAC process used here is not ordinarily accessible for astronomy at optical frequencies, which usually measures intensities. The IAC can be thought of as the extension of FAC methods to light curves (i.e., flux versus time). The IAC finds application in many areas of physics, such as the characterization of ultrashort optical pulses, the detection of weak optical pulsars (Leeb et al. 2015), interstellar scintillation of quasars (Rickett et al. 2002), and measuring stellar rotation periods from *Kepler* light-curve data (McQuillan et al. 2014).

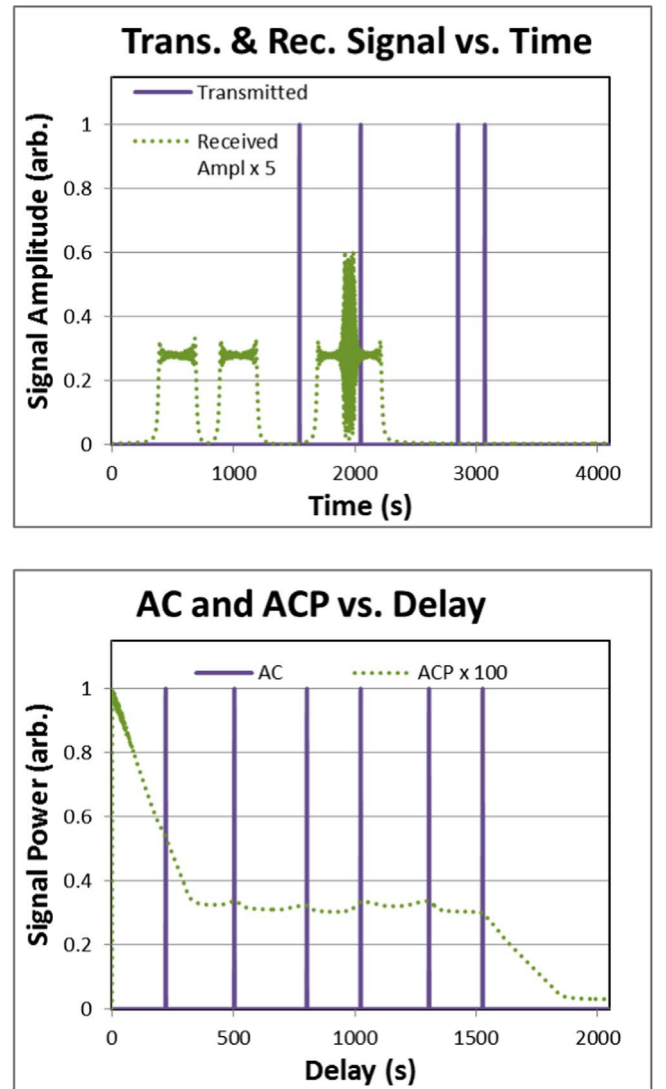


Figure 2. Transmission and reception of a coherent pulsed signal after passage through the interstellar medium for 1600 yr. The left panel compares a baseband copy of the transmitted electric field amplitude at the transmitter (lavender lines) and receiver (green dots). On the right, we plot the autocorrelation of the received electric field (FAC; lavender lines) and autocorrelation of intensity (IAC; dots) for the signal. The repetitive signal is detectable in both FAC and IAC.

Incoherent signals can be detected by IAC even when FAC fails to find them. It is closely related to the method of synchronous averaging of power used in pulsar searches. While the basic principles behind IAC are not new in radio astronomy, we briefly describe it as a comparison to FAC.

2.1. Archetypal Signal Motivating This Work

Almost all modes of human communication are fundamentally symbolic, with symbols repeating in a complex message. This campaign attempts to find signals containing at least some repetitive periodic structure. An archetypal signal here is the wireless Ethernet protocol. Ethernet uses a binary alphabet of symbols to represent arbitrary information. At the hardware level, each symbol is represented by a particular electromagnetic waveform in the radio-frequency band. Such signals are transmitted and, in principle, can escape to great distances from the Earth.

⁷ For example, information encoded using a finite alphabet of symbols with repeating elements at more or less random delays.

⁸ In this discussion, “coherent” pulses are defined as having strong correlation between separate pulses. That is, pulses in the train have identical electric field waveforms.

A distant astronomer with a radio telescope and sufficient sensitivity can detect the transmitted data stream as broadband power arriving from the direction of Earth. Since many natural sources generate broadband power, the artificial nature of the signal might be overlooked. Alternatively, if the astronomer employs an FAC detector, the signal’s artificial nature is immediately evident. The FAC detectors are well suited to identify a host of protocols that transmit information using a finite alphabet of symbols.⁹

2.2. Signal Types

In SETI searches at the ATA, we identify a few archetypal quasi-stationary signal waveforms.

- (A) *Narrowband*. This is a nearly sinusoidal signal where the coherence time is of order 100 ms or longer. In the workhorse implementation called SETI on ATA (SonATA), such signals may carry up to 10 bits s⁻¹ of information. We refer to this method as “conventional SETI.”
- (B) *Wideband power detection*. With an interferometer like the ATA, it is straightforward to capture “snapshots” of the sky covering many square degrees. These snapshot images can be compared across time periods from seconds to hours, or even longer. Such power intensity images may be examined for point sources that could be associated with ET transmitters or other unexpected radiation.
- (C) *Cyclostationary*. A finite alphabet of radio waveforms representing symbols is transmitted in a time series. Then, FAC is sensitive to any pair of like symbols, repeated at specific delays. Cyclostationary is often used in satellite communication implementing error correction (Gardner & Spooner 1992; Leshem et al. 2000; Morrison 2011, 2012). Message information might be encoded in the transmission center frequency, time delay, or signal phase. When substantial galactic dispersion is present, such symbols will generally overlap in time (see dispersed pulses in Figure 2), which significantly impacts signal discovery in IAC but has little impact on signal detectability with FAC.
- (D) With phase modulation, an alphabet may be constructed from a single symbol multiplied by an overall phase factor. With such alphabets, all symbols correlate with all other symbols (see, e.g., the GPS example in Harp et al. 2010a). However, destructive interference between correlations of different symbol pairs can dilute FAC sensitivity. One solution to this problem is described in Morrison (2012), where a separate computation is performed for each symbol period and the correlation magnitudes are summed incoherently (rather than as complex numbers in ordinary FAC). We do not adopt that method here because it requires several orders of magnitude greater computation time than FAC and was not feasible here.

As the number of symbols in the alphabet grows, FAC sensitivity is also diluted, since the average density of like symbols is reduced. This effect does not

substantially alter the conclusions of this paper.

On Earth, cyclostationary signals that contain no extrinsic information (same symbol repeated over and over) are sometimes used in radar applications (e.g., Arecibo planetary radar) to generate a controlled wide-bandwidth signal. If such a signal were discovered in SETI, it would still be conspicuously artificial and of interest.

(E) Amplitude Modulation (AM)

- (a) *Direct transmission, as with broadcast radio*. Compared to frequency or phase modulation, AM is more prone to errors caused by noise and fading.
- (b) *Receive, delay, and transmit*. One suggestion is that ET may take advantage of a strong natural source to enhance detectability. For example, ET can set up a transmitter on a line of sight between Earth and a quasar. Then, ET collects the quasar signal, amplifies it, and retransmits a delayed copy toward Earth (Harp et al. 2010a). Information may be embedded in such a signal using a time-dependent delay.
- (c) *Source modulation*. Direct AM of an astronomical source might be accomplished by modulating or pumping the source itself. As proof of the principle, Weisberg et al. (2005) identified a maser source that is modulated by a pulsar. Since the light-crossing time of the smallest masers is on the order of hundreds of s (Boyd & Werner 1972), modulations at shorter timescales indicate a localized pumping source.
- (d) *Other*. The signal modulations above assume that the received signal is approximately stationary over time periods on the order of 100 ms or smaller. Of course, an infinity of other signal types exist, including nonstationary signals that might be picked up with our autocorrelation detectors below. This is not a problem, since any signal we find has a high likelihood of being artificial.

2.3. The Sensitivity of Various Detectors

We consider a single polarization system where the telescope voltages are digitally sampled and a total of N_s samples are gathered in the observation. The minimum total power P_t for a 1σ detection of a signal is proportional to the telescope’s system equivalent flux density (SEFD), that is, when the astronomical flux density is equal to the system noise power. More precisely,

$$P_t = \frac{(\text{SEFD})}{\sqrt{N_s}}, \quad \text{where} \quad \text{SEFD} = \frac{2\eta k_B T_{\text{sys}}}{\eta_{\text{eff}} A}, \quad (1)$$

$\eta < 1$ is the power-loss factor associated with digitization, k_B is Boltzmann’s constant, A is the total collecting area, and $\eta_{\text{eff}} < 1$ is the aperture efficiency, or the fraction of A that is captured by the receiver in the combined optical system. At the ATA, $\eta_{\text{eff}} = 0.6$ (Harp et al. 2011). For equal signal in two polarizations, P_t is divided by $\sqrt{2}$.

Using measured antenna system temperatures, Table 1 displays the computed sensitivity measures for the various detection algorithms. At four frequencies used in observations, we compute the S/N for a 10 minute observation of a 1 Jy source (e.g., ETI transmitter or a quasar) emitting uniformly over the 7 MHz detector bandwidth in the third column. The

⁹ We note that it would be difficult but not impossible to design a symbolic protocol that evades FAC detection, for example, a BPSK pattern for each letter and regular inversion of the meaning of positive and negative phases with time. Some satellites use this method to eliminate a DC bias in the electric field.

Table 1
Detection Thresholds for Various Algorithms Assuming 600 s
at 7 MHz Bandwidth, $A_{\text{eff}} = 438 \text{ m}^2$

f (GHz)	T_{sys} (K)	S/N 1 Jy Source	1σ Wide- band Detectable Flux (Jy)	1σ Narrow- band Detect- able Flux in 1 Hz bin (Jy)	1σ FAC, Detectable Flux (Jy)
1.43	80	129	0.009	27	0.037
3.04	120	86	0.014	40	0.054
6.667	95	108	0.011	32	0.043
8.4	137	75	0.016	45	0.063
f	T_{sys}	S/N	The ratio of total power at receiver for equivalent detectability		
1.43	80	129	2000	1	10,000

fourth column shows the flux of a source detectable at 1σ for a total power measurement of a wideband signal. For a narrowband signal, the fifth column shows the minimum detectable flux in a 1 Hz bin. Using FAC and IAC detectors and under the favorable assumptions of Gaussian noise (Fano 1951) and that the sample period is commensurate with the symbol period, the sixth column applies. The computed sensitivities were verified with detailed simulations.

The fourth column in Table 1 shows the power detection threshold for a signal whose bandwidth $\text{BW}_{\text{signal}} \geq \text{BW}_{\text{detector}}$. The analogous detection threshold for a very narrowband signal is larger by a factor of $\sqrt{N_{\text{chan}}}$, where N_{chan} is the number of channels across the detector bandwidth. This is because all the power in the threshold wideband signal must be transmitted in a single channel. The detection thresholds for a 1 Hz bandwidth signal are shown in the fifth column of Table 1 for reference only. When comparing sensitivities of different detectors, the fifth column is the relevant column for an arbitrary MFB, irrespective of the actual transmitted signal bandwidth. The sixth column shows the detection sensitivity of FAC and IAC. The most relevant comparison for the sixth column is the fourth column. We return to this comparison in the discussion section.

In Table 1 (bottom row), we multiply the threshold sensitivities by their effective bandwidth, which allows us to compare total transmitter power for equivalent cases. The ratio of transmitter powers is 1:2000:10,000 for the narrowband, wideband, and FAC, respectively, to generate the same detected signal with each metric. As expected, the narrowband signal, where the recipient knows the signal shape, requires the least total power. The necessary wideband power is larger because of the fact that for each antenna pair, we are correlating two independent measures of the signal, both of which contain uncorrelated noise. The FAC power is larger still, since both the reference and test signals must be present at the same time in a single measurement, leaving less power for either of them.

This paper focuses on FAC as an alternative to the narrowband search for ETI. In the next section, we describe how FAC predicts its relative sensitivity.

2.4. The PS and Two Autocorrelation Detectors

The power spectrum (PS), FAC, and IAC detectors are introduced with notional expressions for their computation as compared with that for the traditional PS in Equations (2), (3), and (4), respectively.

The PS uses an ordinary fast Fourier transform (FFT), and this statistic represents a typical MFB detector¹⁰ where the matching functions are oscillating exponentials. The FAC detector is sensitive to repeating modulations of the electric field. The IAC detector is sensitive to repeating modulations of the received power. Using FAC, AM or constant-amplitude signals with phase or frequency modulation are detectable. Here IAC is sensitive to AM but not constant-amplitude (e.g., phase) modulation. Comparatively, typical CCD detectors for light measure only the received power, after which IAC processing is sometimes possible. Radio measurements are special in that the phase of the electric field can be measured, permitting FAC detection.

The actual digital calculations require subtle corrections that are described in the Appendix. For the given observation time, the number N_s of digitized samples is broken into N_b equal blocks of length M . Each block is processed with an FT, which is then averaged over all blocks:

$$\text{PS}(f) = \sum_{n=0}^{N_b-1} \left| \sum_{m=0}^{M-1} \exp(-i 2\pi f t_m) s(nT + t_m) \right|^2, \quad (2)$$

$$\text{FAC}(\tau) = \sigma_s^{-2} \left| \sum_{l=0}^{M-1} \exp(i 2\pi f_l \tau) \sum_{n=0}^{N_b-1} \exp(-i 2\pi f_l t_m) s(nT + t_m) \right|^2, \quad (3)$$

$$\text{IAC}(\tau) = \sigma_s^{-2} \sum_{l=0}^{M-1} \exp(i 2\pi f_l \tau) \sum_{n=0}^{N_b-1} \left| \sum_{m=0}^{M-1} \exp(-i 2\pi f_l t_m) |s(nT + t_m)|^2 \right|. \quad (4)$$

In Equations (2)–(4), $s(nT + t_m)$ is the value of the sample at point m in the n th block, t_m is the time associated with s measured from the start of the n th block, f_l is the baseband frequency, τ is the time delay measured from the start of the n th block, and σ_s and σ_s^2 are the respective mean square variances of the field and intensity. These equations define the PS, averaged magnitude of sampled FAC, and averaged magnitude of sampled IAC detectors, in that order (note the squaring operation inside FT for IAC). As shown, the AC algorithms are implemented using the Wiener–Khinchin convolution theorem (Wozencraft & Jacobs 1990) with forward and inverse FTs. The units of PS and FAC are power, while IAC is different. With IAC, the fluctuations of the measured power are the “signal” we wish to characterize. The units of IAC are also power, based on this definition of “signal.”

In application, we apply a simple 5σ threshold to the FAC statistic to identify signals that are likely to be engineered. Detection is done by visual inspection of graphs. Yet a visual inspection is helpful to be confident that two radio-frequency interference (RFI) signals have the same source. Also, visual inspection makes it easier to excise artifacts with short delay periods. There were fewer than 200 plots, so it was not difficult. As a function of frequency, approximate 1σ threshold flux values for detection are given in Table 1.

¹⁰ In actual observations, signals that deviate slightly from pure sinusoids are also checked.

Table 2
New Limits on Probability of Repetitive ET Transmitter

Source Type	No. Distinct Sources and Distinct Frequencies	No. Possible Observations 1–10 GHz	P_{Hit}
Distinct source >1 Jy	89	4×10^6	0.05
Exoplanet stars	88	$\approx \infty$	0.05

2.5. Observational Design

The ATA is a dual-polarization 42-element interferometer located in Northern California, comprising 6.1 m dishes and dual-linear polarization feeds that can operate in four simultaneous frequency bands centered anywhere between 1 and 10 GHz (Welch et al. 2009).

The signals from many ATA antennas are delayed and summed in a beam former (Barott et al. 2011). Complex-valued (8-bit real, 8-bit imaginary, hence $\eta \approx 1$) samples from the beam former are collected at a rate of 8.73 MS s^{-1} . An anti-aliasing bandpass filter before the digitizers limits the effective bandwidth to 7 MHz. The phased-array beam diameter can be estimated as $0.1/f$, where f is the observation frequency in GHz. Quasars are effectively point sources for the ATA, and many are more than 100 times more powerful than the background level in the time period over which we perform FAC.

Data collections were made over approximately 14 months (2010 January–2011 March) and a full listing of all targets and observation frequencies is presented in Table 3 in the Appendix. The typical ATA configuration used 25 of the 6.1 m antennas in a phased-array beam on the source of interest. We typically accumulated data for 600 s, for an effective total of $N_s = 4.2 \times 10^9$ samples per observation. Referring to Equation (3), $M = 2^{23}$, or approximately 1 s long. The sampled data from each observation were reduced using Gnu Octave (Eaton et al. 1997) to compute the various statistics.¹¹ All of the source data are freely available in an internet archive (Harp et al. 2010b). Plots of PS and IAC were also generated for reference but not included in the analysis here, since those detectors have been well characterized before.

Many source targets (69) were chosen because they are known to have fluxes >1 Jy. From Table 1, we see that if the entirety of that flux were repetitively modulated, then it would appear with high S/N in this survey. Additionally, sources for examination were chosen as follows. Fifty-nine exoplanets and *Kepler* objects of interest were chosen. Observations of 13 pulsars (flux >1 Jy) and the galactic anticenter were performed based on the hypothesis that ET might broadcast in the direction opposed to a known source in their field of view (FOV) as an aid for our detection of them. Two strong methanol masers ($\gg 1$ Jy at the spectral line) were observed to see if those masers might be artificially modulated. Six O-type stars were chosen to study the hypothesis that advanced extraterrestrials might set up beacons using bright stars as an energy source. Other special pointings include the Sun and Moon for artifact tests, the Earth–Sun Lagrange L4 point (where transmitters might be left in a stable orbit), and the ecliptic North Pole.

Observational frequency bands were selected to have minimal strong RFI and often encompass certain “magic” frequencies, such as the H I line (1.420 GHz), $\sqrt{2}$ H I (2.008 GHz), 2 H I (2.840 GHz), π H I (4.462 GHz), the

methanol maser line (6.667 GHz), and 8.4 GHz, because it is close to the upper limit of ATA’s receivers.

Only positive delays were examined, since the curves are symmetric about zero delay. Inspection was performed over the delay range $1 \times 10^{-4} \text{ s} < \tau < 0.25 \text{ s}$, where the bias due to finite M is limited to no more than a factor of 2. The lower limit is chosen to exclude features due to delays in time of arrival at different antennas in the ATA. The time spacing between plotted delays is the same as for the original sampling, $\Delta\tau = 1.4 \times 10^{-7} \text{ s}$.

Interesting signals were noted, and if those signals appeared in observations of more than one spatial direction, they were identified as a ground- or space-based man-made source.

2.6. Identification and Elimination of Human-generated Signals

It is the goal of this paper to focus attention on detecting technological signals no matter how they are generated. We wish to avoid the tedious work of identifying signals’ specific transmitters, be they radar, cell phone, satellite, etc. Instead, we use direction-of-arrival methods to classify signals as coming from either the vicinity of Earth or farther away. Using these methods, we can reliably eliminate signals from human transmitters out to about 10% of the orbit of the Moon without any prior knowledge of spectrum usage. This is important, since there is no part of the radio spectrum free from human interference. Since public documentation regarding most transmitters is spotty at best, it is impossible to rule out most signals by any means other than direction of arrival.

3. Results

We demonstrate the utility of FAC detection with a few examples of (interfering) signals detected in this survey in Figure 3. Figure 3(A) shows a fiducial observation taken in the direction of a known spacecraft beyond lunar orbit (*Deep Impact*) in the frequency range of its communication downlink. This 35 Jy signal¹² is exactly the type of signal we hope to observe. Panels (B) and (C) show an example of an unidentified 7 Jy signal that appeared in multiple pointings and is hence identified as interference. Panel (D) shows how transmission from strong satellites (in this case, the *Geostationary Operational Environmental Satellites* (GOES)) generates interfering (but not imaging) signals at 3 Jy,¹³ even when the telescope is not pointed at them.

Panel (E) shows another unidentified 2 Jy signal, which we labeled as interference because we deem it unlikely that an extraterrestrial transmitter would coincidentally repeat at such a round number (10.000 ms) in Earth units (also seen in more

¹² Effective flux if spread over the full 7 MHz bandwidth of our observations, computed with Table 1 and cross-checked against an earlier DSN measurement: https://descanso.jpl.nasa.gov/DPSummary/di_article_cmp20050922.pdf.

¹³ A GOES satellite uses a 7 W transmitter, an antenna with 11 dB gain, and a typical downlink bandwidth of 100,000 Hz. Therefore, in its frequency of emission, it has a flux density $>1,000,000$ Jy. The measured antenna far-out sidelobes result in approximately 40 dB of suppression (Harp et al. 2011), so the residual signal we see is well within our expectations.

¹¹ Source codes available upon request.

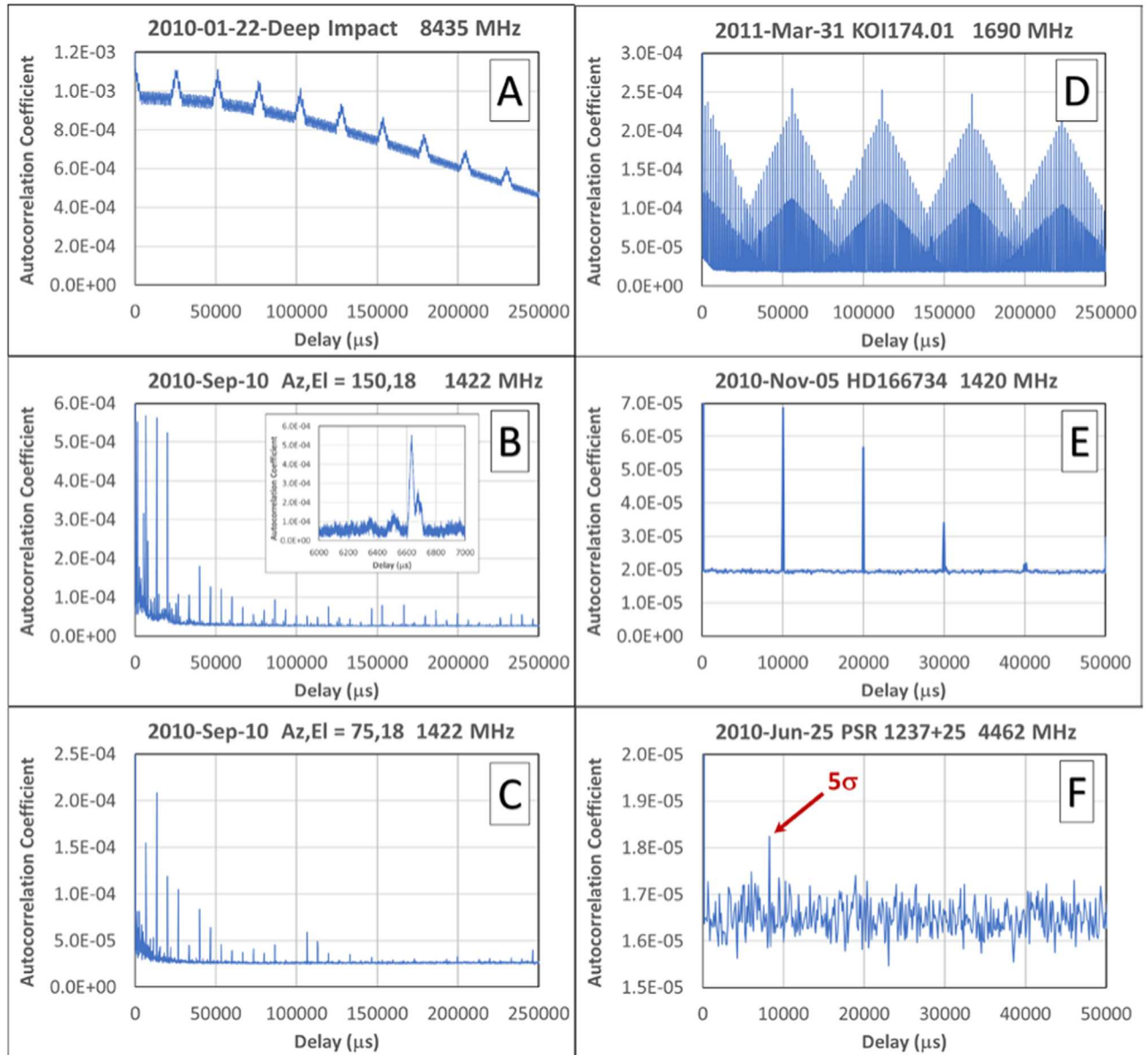


Figure 3. The FAC plots of power as a function of delay on various sources. (A) *Deep Impact* spacecraft in downlink transmission band. (B) and (C) Unexpected interfering signal observed in multiple pointing directions. The inset in panel (B) shows a blowup of the delay region around $6500 \mu\text{s}$. (D) While pointed at a *Kepler* object of interest, an observation at 1690 MHz shows signal in the frequency range of *GOES*, even though all *GOES* satellites were far from the pointing direction. (E) Observed while pointed at a blue supergiant star, the signal period of 10.000 ms is identified as human-generated due to its close alignment with Earth-based time units. (F) While pointed at a pulsar, one of the smallest signals in this paper is detected. Although this too is interference, this plot gives an impression of the S/N obtained in these measurements.

than one direction). Panel (F) shows a weak unidentified signal near the left-hand side with power at our 5σ detection limit (0.32 Jy for this frequency). This signal was observed in multiple pointing directions.

Taking a closer look, the signal in panels (B) and (C) occurs right in the so-called protected radio astronomy band for the H I line. This signal was not visible in IAC, indicating that it is probably phase-modulated. The FAC signal was observed in 7 MHz bands from 1400 to 1470 MHz with approximately uniform power. From this, it is easy to understand why there was no detectable feature in the PS for this signal. Also, because the source of this signal does not resolve to a point on the sky, even a repetitive signal as strong as this is not easily detected in ordinary interferometer observations and went undetected at the ATA for nearly a decade.

We estimated the coherence time of the signal in panels (B) and (C) by computing the statistic using different sample block lengths M but keeping all of the data. The first FAC peak had a maximal plateau for M corresponding to block times greater than 140 ms , while smaller M resulted in a smaller peak. This plateauing behavior indicates that the repetition period is drifting slowly during the observation, changing by the delay of a single sample ($1.2 \mu\text{s}$) in about 140 ms . This demonstrates that we can detect repetitive signals, even if they are weakly nonstationary.

The origin of this signal has not been identified, nor do we speculate on its origin. This study shows how interfering signals are distinguished from true ETI transmissions using direction-of-arrival estimation. This is important; while some interfering sources can be identified with known transmitters, it

is more often the case that the frequencies of such human-generated signals do not correspond with any cataloged source of radiation. Interfering signals are ubiquitous below 5 GHz, and once identified as interference, there is no need for further investigation.

The interesting signal in panel (D) shows how satellite communications can generate interference in FAC observations. We intentionally observed in the transmission band of the *GOES* weather satellites while pointing far away from any of those satellites. Such strong satellite transmissions make radio observations impossible at frequencies where they occur.

Panel (F) is provided to highlight the background noise level of all observations. Because the correlations are computed over a finite period, we expect an average autocorrelation coefficient of $\sim 10^{-5}$, even when the input data contain only noise.

A summary of all of the observational results is as follows. We found 10 distinct signals in FAC that had no counterparts in PS. At least 10 times as many unique signals were observed in the power spectra, which indicates that today, interfering signals are more likely to be narrowband than repetitive. All unidentified signals were observed multiple times and in different pointing directions, indicating that they arise from terrestrial/satellite communications. No unidentified FAC signal was observed with a center frequency above 5 GHz. This indicates very little RFI over the entire upper half of the terrestrial microwave window (~ 1 –10 GHz), frequencies where new future SETI observations will be least impacted.

These examples demonstrate a couple of points: (1) FAC is demonstrated to detect repetitive signals that will not be found in a conventional SETI search, and (2) FAC is a good detector for local RFI that may be difficult to characterize otherwise. We do not know of another radio observatory that uses FAC as a means of identifying RFI, and we suggest that this approach may be useful elsewhere.

4. Analysis

Now we consider the research question,¹⁴ “What is the highest probability for the existence of true repetitive ETI signal that is compatible with our results?” We emphasize that since this is the first substantial survey looking for constant-power repetitive signals, we have little *a priori* knowledge about this question. This survey provides new limits on the probability of observing a repetitive signal in Table 2.

4.1.1. Hypothesis 1

We hypothesize that most previously discovered strong radio sources with flux >1 Jy are constantly modulated with a repeating pattern either directly by extraterrestrials or due to some heretofore unknown physics.

The total population of possible independent observations of all sufficiently strong sources can be estimated as follows. We refer to the NRAO VLA Sky Survey (Condon et al. 1998), which used the VLA to image and identify sources of continuum radiation from most of the sky (except near the South Pole). The NVSS reports more than 2000 sources with flux greater than 1 Jy. Multiplying by the solid angle of the sky divided by the fractional solid angle observed in the survey (and including strong masers, etc.), we estimate the existence of about 2700 sources with flux ≥ 1 Jy. The frequency search

window, 1–10 GHz, can be divided into 1286 independent 7 MHz ranges, as are used here. The number of similar observations required to survey every 1 Jy source from 1–10 GHz is about 4×10^6 .

Combining observations of bright quasars, pulsars, and masers into a single group, we have 89 independent observations on 23 sources >1 Jy. We assume a uniform distribution of repetitively modulated sources in position and frequency. We call the probability that a signal will be detected in any one trial p_{hit} , and the converse probability that no signal is detected $p_{\text{miss}} = 1 - p_{\text{hit}}$. What value of p_{hit} is consistent with our observations at a 99% confidence level? We write

$$P(89 \text{ misses}) = (1 - p_{\text{hit}})^{89} > 100\% - 99\% = 1\%. \quad (5)$$

Solving for hit probability gives $p_{\text{hit}} < 5\%$, or no more than one in 20 sources are being modulated. If we wished to decrease p_{hit} to be less than one in a million, we would require about 4 million negative observations. We set this as an aspirational goal.

It is worth noting that our entire survey severely under-samples the full source search space in the frequency range of 1–10 GHz, where the source modulation may be present (sampling 89 frequency samples out of 4 million). Therefore, our probability estimates here and below should be greeted with some skepticism. The reason we include numerical estimates at all is that we wish to establish limiting values that can be used for comparison in future surveys.

We reiterate this result including all caveats. Of the estimated ~ 2700 radio sources in the sky with flux >1 Jy at 1420 MHz and in the radio frequency range 1–10 GHz, no more than 5% of them might bear (either natural or intentional) repetitive modulation with repeat periods in the range $1 \times 10^{-4} \text{ s} < \tau < 0.25 \text{ s}$.

4.1.2. Hypothesis 2

We suppose that most stars harboring exoplanets are sending repetitive signals. As we now know that most stars harbor exoplanets, this distinction is not as important as we once thought.

With 88 distinct observations, the math is almost identical to that for hypothesis 1. We conclude that at a 99% confidence level, no more than 5% of such stars are actively transmitting repetitive signals that are detectable in this survey.

Finally, another result worthy of comment: the L4 Lagrange point showed no evidence for an artifact transmitting detectable signals in three observations at 1420, 2008, and 3991 MHz.

4.2. Number of Signal Waveforms Probed by Narrowband versus FAC

Given M samples, it is always possible to represent an arbitrary waveform with a basis of M test waveforms. But when searching for signals, we wish to choose a basis set that concentrates all the signal power into a small number of basis functions so that they stand out above the noise. To illustrate this point, consider that a very narrow pulse spreads equal power across every bin in a PS. In the presence of noise, PS is therefore a poor pulse detector. But a pulse basis, where each basis function is merely a linear combination of sinusoids, will readily detect pulsed signals. Different detectors are more or

¹⁴ A more expansive description of our research hypotheses is given in the Introduction.

less sensitive to different linear combinations of the same set of basis signals.

Given M time-series samples, it is interesting to compare the number of different waveforms that can be tested by PS and FAC. Neglecting possible drifts, an FFT is an MFB for the set of all sinusoidal signals with periods between two and M time intervals. Hence, a PS analysis tests an observed time series for $N_W(\text{PS}) = (M - 1)$ potential signal waveforms.

Surprisingly, an FAC analysis probes a larger number of waveforms, despite being derived from the same number of samples. This is because for each FAC period P_n characterized as being n samples in duration, there are a number $(n - 1)$ of linearly independent waveforms that are detected. To avoid overcounting, we establish a lower limit on the number of distinct waveforms $N_W(\text{FAC})$ by choosing only periods where n is a prime number. Thus,

$$N_W(\text{FAC}) > (2 + 3 + 5 + 7 + \dots + M - 1) \\ \approx \int_2^{M-1} dx \frac{x}{\ln(x)} > M^{7/4} > N_W(\text{PS}), \quad (6)$$

where the integral takes advantage of the prime number theorem. The power law $M^{7/4}$ is an empirical fit that works well for $M < 2^{23}$, the number used here. Hence, for M samples, FAC tests for more waveforms than PS. It is important to be clear in our meaning of the “number of tested waveforms” in this context. Naturally, there really are only M (truly) independent waveforms obtainable from M samples. Here N_W is a measure of the number of distinct waveforms for which FAC concentrates the signal power into just one or a few bins as an aid for signal detection. This is of value only when computing resources are limited. The price paid for added flexibility is that FAC requires a larger S/N than PS to obtain the same fixed threshold of detector sensitivity (see last row in Table 1).

But the real motivation behind FAC detection is that we wish to be sensitive to at least some information-carrying signals, which by definition are not sinusoidal waveforms. Classic and recent theoretical studies of the interstellar medium as a communication channel (Drake 1965; Shostak 1995; Messerschmitt 2012; Messerschmitt & Morrison 2012) suggest algorithms capable of discovering radio signals that contain information, a good example being autocorrelation detection (Drake 1965; Jones 1995; Harp et al. 2010a). As implemented here, autocorrelation is sensitive to signals having arbitrary message content, provided some part of the signal repeats with duration $2 \leq P_n \leq M/4$.

It may be true that somehow, the spectrally pure signal (sinusoid) is strongly favored by builders of ET transmitters over any other signal type, possibly because it mimics natural spectral-line sources. The FAC is not at all sensitive to such beacons, and the traditional SETI narrowband search is the optimal. However, there are some downsides to sinusoidal signals. The first is that a pure sinusoid carries only one bit of information: that a transmitter exists. Furthermore, it has been argued (Messerschmitt 2012) that sinusoidal signals are less resistant to interference and multipath (time-variable scintillation-induced) fading than, say, a spread spectrum signal that is repetitively modulated. One last argument against sinusoidal beacons is that most Earth-based radio communications are rapidly converging on spread spectrum signals.

4.3. Sensitivity and Choice of Observation Targets

One argument favoring MFB detectors over any other is that they achieve the theoretical limit for sensitivity to a specific waveform. For a fixed transmission power, waveforms associated with a matched filter can be detected from the greatest distance, R_{max} . The spherical volume centered on Earth, including all transmitter positions detectable at some threshold, is largest for the largest values of R_{max} . In a blind search, this puts FAC at a great disadvantage compared to PS, since transmitters must be closer to be detected by FAC.

This is why approximately half of our survey was directed toward known continuum sources emitting a high flux. In such cases, we already know that there is enough power arriving from the source to trigger an FAC detector if that power were modulated. By selecting bright targets, the distance between the source and Earth becomes irrelevant. This leads to the conclusion that FAC detection has the greatest value when applied to bright sources but substantially less value than PS for a blind search or survey of the sky.

4.4. An Improved FAC Search Design for the Future

We have shown that FAC detection probes an immense region of signal discovery space not observed in conventional SETI campaigns. In designing the next-generation search, we consider two target types: (1) repetition in radiation from known strong sources and (2) repetitive signals from directions where no strong flux is expected.

Targets having known flux should be chosen such that they carry sufficient flux to trigger FAC detection. The minimum detectable flux in this paper is ~ 1 Jy, which is well above the threshold for FAC at the ATA. The VLA archives contain measurements of many sources above -20° decl. Using such archive data may one day allow an expansion of this survey for repetitive signals.

We speculate that there might be a class of sources that do not show substantial flux over very wide bandwidths (~ 100 MHz) but do show flux over modest bandwidths (Hz to tens of MHz). An examination of Table 1 shows that such sources would be more easily discovered using a total power-imaging survey than with direct application of FAC processing. This is because the sensitivity to raw power is greater than the sensitivity to FAC.

From these considerations, we propose that the next-generation SETI detection system should include three components: (1) a total power-imaging survey covering all frequencies between 1 and 10 GHz, (2) a conventional narrowband SETI detector, and (3) an autocorrelation detector running in parallel and even using the same data streams as for items (1) and (2).

4.5. Computation of FAC from Correlator Output

The FAC can be applied to any observed power spectral data. And besides single-dish or phased-array beam data, we believe we are the first to point out that radio interferometer data for imaging can be an excellent source of data for archival FAC searches. Large archives of untested data are available from many telescopes, including the VLA, Westerbork, SRT, GMRT, MeerKat, and ASKAP at centimeter wavelengths; LOFAR and other low-frequency arrays; and at high frequencies with ALMA.

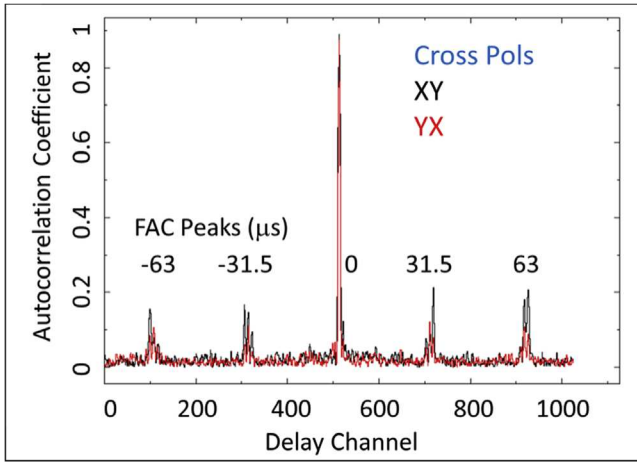


Figure 4. Demonstration of the FAC technique using an imaging correlator as a detector. Since most modern interferometer telescopes use correlators, this method has wide application.

Most interferometers designed for radio imaging employ correlators that produce spectral data. Visibilities are integrated over time periods typically from seconds to minutes and then stored for subsequent image generation. Such data sets are well suited for FAC because a delay measure can be computed from each of hundreds to thousands of correlation spectra. One can implement RFI rejection by comparing delay measures across all antenna pairs, since for a point source in the FOV, a repetitive ET signal should have the same FAC in every correlation, whereas RFI coming from outside the FOV will not be constant across correlations.

We demonstrate this approach using data from a joint experiment between the ATA and the Arecibo Observatory (Figure 4). The Arecibo planetary radar was pointed toward the center of the Moon, and transmissions using binary phase-shift keying (BPSK) were sent with a transmitter bandwidth of 27 MHz. The chip (symbol) duration was $0.5 \mu\text{s}$, and the same string of 63 symbols was sent over and over. The signal had no AM (only phase), with a repetition rate of $31.5 \mu\text{s}$.

The ATA was pointed toward the Moon with an FOV much larger than the Moon’s diameter. Arecibo transmitted at 2380 MHz with 250 kW of power. Neglecting specular reflection, we assume that this power was 100%¹⁵ diffusely scattered into a hemisphere, and taking into account the distance between the Earth and Moon, the proportion arriving in the ATA was less than 10^{-7} of the transmitted signal. The ATA filling factor is less than 1%, so the signal entering our array aperture was about 2.5×10^{-7} W; it was so strong that it was difficult to attenuate the signal enough to prevent overdriving the receivers.

Because the radar is circularly polarized, choosing different polarizations on antenna pairs (XY or YX, cross-polarization) captures the reflected polarized signal (shown) and isolates the radar signal from background radiation. The XX, YY spectra (not shown for brevity) showed very similar features. Visibility spectra from the Moon-bounce observation were Fourier transformed to the delay domain and then summed coherently. Clear peaks are seen in Figure 4, with delays corresponding to the $31.5 \mu\text{s}$ repeat time of the transmitted BPSK signal.

Compared to the 2×10^6 delay values examined in this survey, FAC observations with a correlator are limited in delay. The ATA correlator has a fixed number (1024) of spectral bins independent of the spectral bandwidth. Thus, no more than 512 delay values may be computed. Since correlators generally integrate over periods measured in seconds (possibly milli-second periods in the next generation), we are limited to a maximum delay equal to half the inverse bin width. At the ATA, the maximum delay values for 104–6.5 MHz settings are $4.8\text{--}77 \mu\text{s}$, respectively. Hence, FAC signal searches are optimized when using the maximum number of channels in the correlator, and different delay ranges can be covered with different correlator observation bandwidths.

4.6. Beyond Detection of FAC Signals

The relationship between artificial repetition and real sky structure in correlator images deserves further comment. When a point source is within the FOV, it generally appears as regular oscillations or fringes within the visibility bandwidth for every antenna pair.¹⁶ The fringe period versus frequency depends on the orientation and distance between the antenna pair (baseline), and it is stationary on all baselines when the interferometer is phased up on the source. We call these structure fringes because they originate from source structure in the FOV.

Repetitive sources introduce what we call delay fringes into the visibility spectra. Unless mitigated, delay fringes generate spurious structure in the radio image. Unlike structure fringes, delay fringes have the same oscillation period in every visibility, independent of the antenna positions. The latter property allows us to distinguish real spatial structure from signal repetition.

Structure fringes show peaks in the delay domain, one for each point source in the image. Sources at phase center peak at zero delay. Sources far from phase center exhibit peaks with a range of positive or negative delays on different baselines.

In comparison, if a repetitive signal (from anywhere) is present, then FAC peaks will appear at the same delay values for all baselines. Because delay fringes transform to a range of differently scaled structure in images, artificial repetitive signals may generate telescope-specific and time-dependent “halos” around the image phase center.

Summing delay fringes over baselines reinforces repetition delay peaks relative to structural delay peaks, at once providing a robust detection scheme for identifying artificial repetitive signals. If these signals are unwanted, their interference peaks may be zeroed out in delay spectra, after which an FT back to the frequency domain can result in improved imaging.

5. Conclusions

This paper reports a novel survey of galactic and extragalactic targets (quasars, supernova remnants, masers, pulsars, stars with known planets, O-type stars, the Lagrange L4 point, etc.) searching for artificially engineered signals bearing repetitive structure. Signal detection was performed using ~ 10 minute observations with 7 MHz effective bandwidth captured to disk and post-processed using autocorrelation of the complex-valued voltage signal.

The scientific outcomes of this survey include the following.

¹⁵ The true reflectivity is about 10% of this.

¹⁶ For discussion, assume that the source bandwidth is greater than the observation bandwidth.

1. Of the known continuum sources with flux >1 Jy at 1420 MHz, no more than one in 20 sources are being modulated.
2. The same is true for stars known to have exoplanets.

When a new probe for extraterrestrial signals is introduced, even a modest survey can add greatly to the human reservoir of knowledge. This paper reports the first search for repetitive extraterrestrial signals, some of which might be hiding “in plain sight” but not detected in ordinary analyses of radio telescope data. This principle is demonstrated by the discovery of heretofore unknown and strong repetitive RFI at the ATA.

We were able to eliminate all observed repetitive signals as candidates for an extraterrestrial signal using direction-of-origin methods alone and without prior knowledge of human transmitters’ frequencies or physical locations. This is generally true for all the SETI performed at the SETI Institute, with the exception of a relatively small number of signals that disappear before their direction of origin can be determined. There were no such cases in the present work.

Finally, we lay the groundwork for a proposed campaign to look for repetitive signals using archived correlator data, especially on known sources with continuum flux at several times the noise floor of the telescope. Such a campaign requires no new observations and can explore all of the sky over a modest range of repetition delays.

The authors gratefully acknowledge Franklin P. Antonio for support of this research. We also thank two anonymous referees for astute comments and helpful discussions that greatly improved the paper during review.

Appendix

A.1. Details of Digital Computation

The actual numerical calculations of PS, FAC, and IAC are rather more complex than the notional Equations (2)–(4). For all statistics, the initial FT is performed on a block of $M = 2^{22}$ samples corresponding to half a second in time. Prior to FFT, the block is shifted to zero mean to eliminate the uninteresting zero frequency feature. The block is then multiplied by a Hanning window. This is a raised cosine function that goes to zero at the edges of the sampled time period and removes many artifacts present in a simple periodogram. After the first block, the latter $M/2$ samples from the first block are retained and concatenated with $M/2$ new samples from the data set. In conjunction with the Hanning window, this overlapping preserves the total power of the sampled data after FFT.

For PS and FAC, we use the sampled electric field values as the starting point for the FFT. After the first FFT, the transformed values are squared to compute the PS. For FAC, the averaged PS is padded with $M/2$ zeros on each end to form an array of length $2M$. This padding prevents mixing of positive and negative delays. The result is passed through an inverse FFT (Weiner–Khinchin theorem) to find the complex-valued autocorrelation statistic. When the signal is stationary, the complex-valued statistic can be averaged over long times. However, this is not always the case (see discussion of Figures 3(A) and (B)). To minimize cancellation to the extent possible, we average the absolute value of the FAC statistic over half-second intervals; hence, it is real and positive-definite at all points with units of power.

As computed, correlation statistics are biased with a smoothly varying envelope, peaking at zero delay and going to zero at maximum delay. We correct (normalize) for this bias by dividing each FAC coefficient by the coefficient for a signal containing pure Gaussian noise over a very long time ($\gg 10$ minutes) and subjected to the same analysis. Although this normalization introduces mild heteroscedasticity, we focus our attention on only the lower 50% of delay values to minimize its effects.

The raw autocorrelation values in the plots of Figure 3 have 2^{21} individual points, much more than can be adequately displayed in a printed plot. To bring the number of points down to a manageable group, the original AC data are binned with a max-pooling method (each point represents the largest of 1024 points in the raw AC data). To give a better impression of the actual point density, we blow up a region around the first peak in Figure 3(B) that includes all of the computed AC values between 6000 and 7000 μs .

The convolution algorithm (Wiener–Khinchin theorem) for FAC is important in this application, as it costs only $2\times$ more computation than for the PS (Harp et al. 2010a). A more sensitive FAC-based algorithm, symbol-wise autocorrelation (Morrison 2012, 2017) might be pursued in future studies but will require $>400,000$ times more computation time than for the campaign presented here.

A.2. Observation Table

A list of all observations collected for this project is given in Table 3. The raw data for these observations are available online (Harp et al. 2010b). Sources with “off” in their name track the path of the stated object but following the real source with a delay of ~ 1 hr.

Table 3
List of Observations for This Study

Source	Coordinate	Type	Freq. (MHz)	Flux (Jy) @obs freq	Date
0136+478	01 36 59 +47 51 29	Quasar	2008	1.7	2010 Dec 24
0136+478	01 36 59 +47 51 29	Quasar	4462	1.9	2010 Dec 17
0136+478	01 36 59 +47 51 29	Quasar	6670	1.9	2010 Dec 12
0228+673	02 28 50 +67 21 03	Quasar	2008	1.2	2011 Jan 7
0228+673	02 28 50 +67 21 03	Quasar	6670	2.0	2010 Dec 12
0744-064	07 44 22 -06 29 36	Quasar	2840	4.7	2010 Jul 2
0834+555	08 34 55 +55 34 21	Quasar	2840	6.8	2010 Jul 2
0834+555	08 34 55 +55 34 21	Quasar	2840	6.8	2010 Dec 24
0834+555	08 34 55 +55 34 21	Quasar	3100	6.6	2010 Jul 22
0834+555	08 34 55 +55 34 21	Quasar	6670	4.4	2010 Dec 17
1347+122	13 47 33 +12 17 24	Quasar	2008	4.6	2010 Dec 24
1347+122	13 47 33 +12 17 24	Quasar	4462	3.0	2010 Dec 24
1347+122	13 47 33 +12 17 24	Quasar	6670	2.7	2010 Dec 12
1733-130	17 33 03 -13 04 50	Quasar	2008	5.1	2011 Feb 4
1733-130	17 33 03 -13 04 50	Quasar	4462	4.8	2010 Dec 17
1733-130	17 33 03 -13 04 50	Quasar	6670	10.1	2010 Dec 12
2038+513	20 38 37 +51 19 13	Quasar	2008	4.9	2011 Feb 4
2038+513	20 38 37 +51 19 13	Quasar	6670	3.4	2010 Dec 17
2206-185	22 06 10 -18 35 39	Quasar	2008	5.8	2011 Feb 4
2206-185	22 06 10 -18 35 39	Quasar	4462	3.9	2010 Dec 17
3c119	04 32 37 +41 38 28	Quasar	2008	7.1	2011 Feb 4
3c119	04 32 37 +41 38 28	Quasar	2840	5.4	2010 Jul 2
3c119	04 32 37 +41 38 28	Quasar	4462	3.9	2010 Jun 25
3c123	04 37 04 +29 40 14	Quasar	2008	39.7	2011 Feb 4
3c123	04 37 04 +29 40 14	Quasar	2840	31.7	2010 Jul 2
3c123	04 37 04 +29 40 14	Quasar	4465	23.6	2010 Jun 25
3c138	05 21 10 +16 38 22	Quasar	2008	7.1	2011 Feb 4
3c138	05 21 10 +16 38 22	Quasar	2840	5.4	2010 Jul 2
3c138	05 21 10 +16 38 22	Quasar	4462	4.0	2010 Jun 25
3c147	05 42 36 +49 51 07	Quasar	2008	18.1	2011 Feb 4
3c147	05 42 36 +49 51 07	Quasar	2840	12.5	2010 Jul 2
3c147	05 42 36 +49 51 07	Quasar	4462	8.6	2010 Jun 25
3c274	12 30 49 +12 23 29	Quasar	2008	3.0	2010 Dec 24
3c274	12 30 49 +12 23 29	Quasar	2840	3.0	2010 Jul 2
3c274	12 30 49 +12 23 29	Quasar	4462	3.0	2010 Dec 24
3c274	12 30 49 +12 23 29	Quasar	6670	3.0	2010 Dec 17
3c279	12 56 11 -05 47 22	Quasar	6670	13.6	2010 Dec 17
3c286	13 31 08 +30 30 33	Quasar	1420	14.9	2010 Oct 15
3c286	13 31 08 +30 30 33	Quasar	2008	12.9	2011 Jan 7
3c286	13 31 08 +30 30 33	Quasar	2008	12.9	2010 Dec 24
3c286	13 31 08 +30 30 33	Quasar	4020	8.4	2010 Oct 8
3c286	13 31 08 +30 30 33	Quasar	6670	6.3	2010 Dec 12
3c295	14 11 21 +52 12 09	Quasar	2008	17.0	2011 Jan 7
3c295	14 11 21 +52 12 09	Quasar	6670	3.0	2010 Dec 12
3c345	16 42 59 +39 48 37	Quasar	2008	7.9	2011 Jan 7
3c345	16 42 59 +39 48 37	Quasar	2008	7.9	2011 Feb 4
3c345	16 42 59 +39 48 37	Quasar	6670	5.5	2010 Dec 12
3c380	18 29 32 +48 44 46	Quasar	2008	10.6	2011 Feb 4
3c380	18 29 32 +48 44 46	Quasar	6670	4.0	2010 Dec 17
3c395	19 02 56 +31 59 42	Quasar	6670	1.2	2010 Dec 17
3c48	01 37 41 +33 09 35	Quasar	1422	16.5	2010 Aug 13
3c48	01 37 41 +33 09 35	Quasar	2008	13.0	2010 Dec 24
3c48	01 37 41 +33 09 35	Quasar	2840	8.9	2010 Jul 02
3c48	01 37 41 +33 09 35	Quasar	4462	5.9	2010 Dec 17
3c48	01 37 41 +33 09 35	Quasar	6670	4.2	2010 Dec 24
3c84	03 19 48 +41 30 42	Quasar	2840	23.6	2010 Jul 2
3c84	03 19 48 +41 30 42	Quasar	4462	23.4	2010 Jun 25
3c84	03 19 48 +41 30 42	Quasar	4462	23.4	2010 Sep 10
3c84	03 19 48 +41 30 42	Quasar	6670	22.1	2010 Dec 17
Blazars					
BL Lacterus	22 02 43 +42 16 40	Blazar	1420	6.1	2010 Oct 15
BL Lacterus	22 02 43 +42 16 40	Blazar	2008	5.9	2010 Oct 15
BL Lacterus	22 02 43 +42 16 40	Blazar	6670	4.2	2010 May 21
BL Lacterus	22 02 43 +42 16 40	Blazar	8200	4.0	2010 Aug 13

Table 3
(Continued)

Source	Coordinate	Type	Freq. (MHz)	Flux (Jy) @obs freq	Date
S5 0716+714	07 21 53 +71 20 36	Blazar	1414	~1.5 varies	2010 Oct 15
S5 0716+714	07 21 53 +71 20 36	Blazar	1420	~1.5 varies	2010 Oct 15
S5 0716+714	07 21 53 +71 20 36	Blazar	1420	~1.5 varies	2010 May 21
S5 0716+714	07 21 53 +71 20 36	Blazar	1422	~1.5 varies	2010 Aug 13
S5 0716+714	07 21 53 +71 20 36	Blazar	1422	~1.5 varies	2010 Aug 13
S5 0716+714	07 21 53 +71 20 36	Blazar	1422	~1.5 varies	2010 Oct 15
S5 0716+714	07 21 53 +71 20 36	Blazar	1426	~1.5 varies	2010 Aug 13
S5 0716+714	07 21 53 +71 20 36	Blazar	1427	~1.5 varies	2010 Oct 15
S5 0716+714	07 21 53 +71 20 36	Blazar	1432	~1.5 varies	2010 Aug 13
S5 0716+714	07 21 53 +71 20 36	Blazar	1435	~1.5 varies	2010 May 21
S5 0716+714	07 21 53 +71 20 36	Blazar	1459	~1.5 varies	2010 Oct 22
S5 0716+714	07 21 53 +71 20 36	Blazar	3086	~1.5 varies	2010 Dec 17
S5 0716+714	07 21 53 +71 20 36	Blazar	6670	~1.5 varies	2010 Oct 22
S5 0716+714	07 21 53 +71 20 36	Blazar	8200	~1.5 varies	2010 May 07
0954+658	09 58 47 +65 33 55	Blazar	1432	~1.3 varies	2010 Oct 15
0954+658	09 58 47 +65 33 55	Blazar	8200	~1.3 varies	2010 Oct 22
Supernova Remnants and Masers					
taua	05 34 32 +22 00 58	SNR	2008	1110.0	2010 Aug 13
taua	05 34 32 +22 00 58	SNR	1420	1110.0	2010 May 7
taua	05 34 32 +22 00 58	SNR	2840	1110.0	2010 Oct 15
casa	23 23 27 +58 48 28	SNR	2008	1547.3	2010 Aug 13
casa	23 23 27 +58 48 28	SNR	4462	885.9	2010 Oct 15
casa	23 23 27 +58 48 28	SNR	6670	701.1	2010 Aug 13
w51	19 23 44 +14 30 33	Maser	6670	850 peak	2010 May 7
w3oh	02 27 04 +61 52 25	Maser	6670	3741 peak	2010 Mar 26
w3oh	02 27 04 +61 52 25	Maser	6670	3741 peak	2010 Apr 2
w3oh	02 27 04 +61 52 25	Maser	6670	3741 peak	2010 May 7
				@1400 MHz	
Crab	05 34 32 +22 00 52	Pulsar	2008	12.6	2011 Feb 4
Crab	05 34 32 +22 00 52	Pulsar	1420	12.6	2010 Mar 26
Crab	05 34 32 +22 00 52	Pulsar	1420	12.6	2010 Oct 15
Crab	05 34 32 +22 00 52	Pulsar	2600	12.6	2010 Mar 9
Crab	05 34 32 +22 00 52	Pulsar	4462	12.6	2010 May 7
Crab	05 34 32 +22 00 52	Pulsar	1420	12.6	2010 May 7
Crab	05 34 32 +22 00 52	Pulsar	4462	12.6	2010 Jun 25
psrb0329+54	03 32 59 +54 34 44	Pulsar	1420	1.8	2010 May 7
psrb0329+54	03 32 59 +54 34 44	Pulsar	1420	1.8	2010 May 21
psrb0329+54	03 32 59 +54 34 44	Pulsar	611	1.8	2011 Mar 4
psrb0450+55	04 54 08 +55 43 42	Pulsar	4462	0.3	2010 Jun 25
psrb0809+74	08 14 59 +74 29 06	Pulsar	4462	0.0	2010 Jun 25
psrb0809+74	08 14 59 +74 29 06	Pulsar	1420	0.0	2010 May 14
psrb0823+26	08 26 51 +26 37 24	Pulsar	4462	0.1	2010 Jun 18
psrb0823+26	08 26 51 +26 37 24	Pulsar	4462	0.1	2010 Jun 25
psrb0950+08	09 53 09 +07 55 36	Pulsar	4462	3.2	2010 Jun 18
psrb0950+08	09 53 09 +07 55 36	Pulsar	4462	3.2	2010 Jun 25
psrb1133+16	11 36 03 +15 51 04	Pulsar	4462	0.9	2010 Jun 25
psrb1237+25	12 39 40 +24 53 49	Pulsar	4462	0.4	2010 Jun 25
psrb1937+21	19 39 39 +21 34 59	Pulsar	1420	0.3	2010 Nov 5
Stars—Including <i>Kepler</i> Exoplanets, O stars					
koi001	13 12 44 -31 52 24	Exoplanet	4462	<1	2010 Sep 10
koi044	22 53 13 -14 15 13	Exoplanet	4462	<1	2010 Mar 26
koi051	09 34 50 -12 07 46	Exoplanet	4462	<1	2010 Sep 10
koi054	10 58 28 -10 46 13	Exoplanet	4462	<1	2010 Sep 10
koi060	03 32 55 -09 27 29	Exoplanet	1420	<1	2010 Mar 19
koi062	12 44 20 -08 40 17	Exoplanet	4462	<1	2010 Sep 10
koi071	11 35 52 -04 45 21	Exoplanet	4462	<1	2010 Sep 10
koi072	22 09 40 -04 38 27	Exoplanet	4462	<1	2010 Mar 26
koi073	09 56 06 -03 48 30	Exoplanet	4462	<1	2010 Sep 10
koi076	12 19 13 -03 19 11	Exoplanet	4462	<1	2010 Sep 10
koi080	13 12 43 -02 15 54	Exoplanet	4462	<1	2010 Sep 10
koi081	10 42 48 -02 11 01	Exoplanet	4462	<1	2010 Sep 10
koi084	11 24 17 -01 31 44	Exoplanet	4462	<1	2010 Sep 10
koi096	11 45 42 +02 49 17	Exoplanet	4462	<1	2010 Sep 10




Table 3
(Continued)

Source	Coordinate	Type	Freq. (MHz)	Flux (Jy) @obs freq	Date
koi097	11 26 46 +03 00 22	Exoplanet	4462	<1	2010 Sep 10
koi112	12 13 29 +10 02 29	Exoplanet	4462	<1	2010 Sep 10
koi117	10 18 21 +12 37 15	Exoplanet	4462	<1	2010 Sep 10
koi118	13 28 26 +13 47 12	Exoplanet	4462	<1	2010 Sep 10
koi119	11 46 24 +14 07 26	Exoplanet	4462	<1	2010 Sep 10
koi125	13 12 19 +17 31 01	Exoplanet	4462	<1	2010 Sep 10
koi126	10 10 07 +18 11 12	Exoplanet	4462	<1	2010 Sep 10
koi127	23 18 47 +18 38 45	Exoplanet	3100	<1	2010 Jul 22
koi130	04 42 56 +18 57 29	Exoplanet	1420	<1	2010 Mar 19
koi133	09 23 47 +20 21 52	Exoplanet	3100	<1	2010 Jul 22
koi134	00 44 41 +20 26 56	Exoplanet	4462	<1	2010 Mar 26
koi144	00 39 21 +21 15 01	Exoplanet	1420	<1	2010 Mar 19
koi150	02 04 34 +25 24 51	Exoplanet	4462	<1	2010 Mar 26
koi155	11 42 11 +26 42 23	Exoplanet	4462	<1	2010 Sep 10
koi160	08 52 37 +28 20 02	Exoplanet	1420	<1	2010 Mar 19
koi172	00 20 40 +31 59 24	Exoplanet	4462	<1	2010 Mar 26
koi191	22 57 47 +38 40 30	Exoplanet	3100	<1	2010 Jul 22
koi195	10 59 29 +40 25 46	Exoplanet	4462	<1	2010 Sep 10
koi201	10 22 10 +41 13 46	Exoplanet	4462	<1	2010 Sep 10
koi201	10 22 10 +41 13 46	Exoplanet	3100	<1	2010 Jul 22
koi202	01 36 48 +41 24 38	Exoplanet	1420	<1	2010 Mar 19
koi208	06 04 29 +44 15 37	Exoplanet	3100	<1	2010 Jul 22
koi211	19 28 59 +47 58 10	Exoplanet	1420	<1	2010 Sep 24
koi211	19 28 59 +47 58 10	Exoplanet	4462	<1	2010 Oct 1
koi216	07 48 07 +50 13 33	Exoplanet	3100	<1	2010 Jul 22
koi219	14 56 55 +53 22 56	Exoplanet	1420	<1	2010 Sep 24
koi219	14 56 55 +53 22 56	Exoplanet	4462	<1	2010 Oct 1
koi220	13 34 02 +53 43 42	Exoplanet	4462	<1	2010 Sep 10
koi221	15 35 16 +53 55 20	Exoplanet	1420	<1	2010 Sep 24
koi221	15 35 16 +53 55 20	Exoplanet	4462	<1	2010 Oct 1
koi222	18 10 32 +54 17 12	Exoplanet	4462	<1	2010 Oct 1
koi225	07 21 33 +58 16 05	Exoplanet	4462	<1	2010 Oct 1
koi226	15 24 55 +58 57 57	Exoplanet	4462	<1	2010 Oct 1
koi227	08 18 22 +61 27 38	Exoplanet	4462	<1	2010 Oct 1
koi228	08 40 13 +64 19 41	Exoplanet	4462	<1	2010 Oct 1
koi231	12 05 15 +76 54 20	Exoplanet	4462	<1	2010 Sep 10
koi233	05 22 33 +79 13 52	Exoplanet	3100	<1	2010 Jul 22
koi236	13 00 03 +12 00 07	Exoplanet	4462	<1	2010 Sep 10
Gliese 581	15 19 27 -07 43 20	Exoplanet	1420	<1	2010 Oct 1
Gliese 581	15 19 27 -07 43 20	Exoplanet	4462	<1	2011 Jan 28
Gliese 581	15 19 27 -07 43 20	Exoplanet	4462	<1	2010 Oct 1
koi04	19 02 28 +50 08 09	Exoplanet	1418	<1	2010 May 14
koi04	19 02 28 +50 08 09	Exoplanet	1420	<1	2010 Jan 22
koi04	19 02 28 +50 08 09	Exoplanet	1420	<1	2010 Mar 19
koi04	19 02 28 +50 08 09	Exoplanet	1420	<1	2010 Mar 19
koi04	19 02 28 +50 08 09	Exoplanet	1420	<1	2010 Apr 2
koi04	19 02 28 +50 08 09	Exoplanet	1420	<1	2010 Sep 24
koi04	19 02 28 +50 08 09	Exoplanet	1420	<1	2010 Nov 5
koi04	19 02 28 +50 08 09	Exoplanet	1420	<1	2010 May 14
koi04	19 02 28 +50 08 09	Exoplanet	1692	<1	2010 Sep 24
koi139.01	19 26 37 +44 41 18	Exoplanet	1690	<1	2011 Mar 31
koi174.01	19 47 18 +48 06 27	Exoplanet	1690	<1	2011 Mar 31
koi268.01	19 02 55 +38 30 25	Exoplanet	1690	<1	2011 Mar 31
koi51.01	19 43 40 +41 19 57	Exoplanet	1690	<1	2011 Mar 31
koi70.03	19 10 48 +42 20 19	Exoplanet	1690	<1	2011 Mar 31
55 Cancri	08 52 36 +28 19 51	OZMA star	1420	<1	2010 Nov 5
zeta Oph	16 37 10 -10 34 02	O star	1420	<1	2010 Nov 5
zeta Oph	16 37 10 -10 34 02	O star	2008	<1	2010 Dec 24
zeta Oph	16 37 10 -10 34 02	O star	2840	<1	2010 Dec 24
zeta Oph	16 37 10 -10 34 02	O star	6670	<1	2010 Dec 17
HD 172175	18 39 04 -07 51 35	O star	1420	<1	2010 Nov 5
HD 166734	18 12 25 -10 43 53	O star	1420	<1	2010 Nov 5
HD 093521	10 48 24 +37 34 13	O star	1420	<1	2010 Nov 5

Table 3
(Continued)

Source	Coordinate	Type	Freq. (MHz)	Flux (Jy) @obs freq	Date
HD 060848	07 37 06 +16 54 15	O star	1420	<1	2010 Nov 5
BD 114586	18 18 03 -11 17 39	O star	1420	<1	2010 Nov 5
Special Pointings					
Sun	N/A	Sun	1414	~1000000	2010 Oct 15
Sun	N/A	Sun	1420	~1000000	2010 Oct 15
Sun	N/A	Sun	1426	~1000000	2010 Oct 15
Moon	N/A	Moon	1420	~10000	2010 Oct 8
Moon	N/A	Moon	1420	~10000	2010 Nov 5
northpole	00 00 00+90 00 00	North Pole	1543	<1	2010 Oct 22
northpole	00 00 00+90 00 00	North Pole	3086	<1	2010 Oct 22
Lagrange-4	Sun-Earth L4	Lagrange point	1420	<1	2010 Oct 8
Lagrange-4	Sun-Earth L4	Lagrange point	2008	<1	2010 Oct 8
Lagrange-4	Sun-Earth L4	Lagrange point	3991	<1	2010 Oct 8
galanticenter	05 45 37 +28 56 10	Galactic anticenter	1420	<1	2010 May 7
galanticenter	05 45 37 +28 56 10	Galactic anticenter	1422	<1	2010 May 7
galanticenter	05 45 37 +28 56 10	Galactic anticenter	3991	<1	2010 May 7
galanticenter	05 45 37 +28 56 10	Galactic anticenter	3991	<1	2010 Oct 8
galanticenter	05 45 37 +28 56 10	Galactic anticenter	4462	<1	2010 May 7
galanticenter	05 45 37 +28 56 10	Galactic anticenter	2008	<1	2010 May 7
galanticenter	05 45 37 +28 56 10	Galactic anticenter	3991	<1	2010 Oct 8
Confirmation Observations (Intentionally Away from Some Particular Source)					
blank06	06 00 00 +40 00 00	Off beam	1422		?
blank06	06 00 00 +40 00 00	Off beam	1427		?
blank18	18 00 00 +70 00 00	Off beam	6670		?
blank18	18 00 00 +70 00 00	Off beam	2008		?
blank	09 18 06-11 54 17	Off beam	2840		?
off EpsilonEridani	03 32 56 +09 27 30	Off beam	1420		?
off EtaAeitis	02 12 48 +21 12 39	Off beam	1420		?
off galanticenter	05 45 37 +33 56 10	Off beam	2008		?
off galanticenter	05 45 37 +33 56 10	Off beam	3991		?
off Gliese581	15 19 27 +07 43 20	Off beam	4462		?
off Gliese581	15 19 27 +07 43 20	Off beam	1420		?
off HD69830	08 18 24 +12 37 56	Off beam	1420		?
off TauCeti	01 44 04 +15 56 15	Off beam	1420		?
Confirmation Observations (surveying RFI at ATA)					
AZEL360-18	fixed az, el	Az sweep	1410		?
AZEL345-18	fixed az, el	Az sweep	1410		?
AZEL330-18	fixed az, el	Az sweep	1410		?
AZEL315-18	fixed az, el	Az sweep	1410		?
AZEL300-18	fixed az, el	Az sweep	1410		?
AZEL285-18	fixed az, el	Az sweep	1410		?
AZEL270-18	fixed az, el	Az sweep	1410		?
AZEL255-18	fixed az, el	Az sweep	1410		?
AZEL240-18	fixed az, el	Az sweep	1410		?
AZEL225-18	fixed az, el	Az sweep	1410		?
AZEL210-18	fixed az, el	Az sweep	1410		?
AZEL195-18	fixed az, el	Az sweep	1410		?
AZEL180-18	fixed az, el	Az sweep	1410		?
AZEL165-18	fixed az, el	Az sweep	1410		?
AZEL150-18	fixed az, el	Az sweep	1410		?
AZEL135-18	fixed az, el	Az sweep	1410		?
AZEL120-18	fixed az, el	Az sweep	1410		?
AZEL105-18	fixed az, el	Az sweep	1410		?
AZEL090-18	fixed az, el	Az sweep	1410		?
AZEL075-18	fixed az, el	Az sweep	1410		?
AZEL060-18	fixed az, el	Az sweep	1410		?
AZEL045-18	fixed az, el	Az sweep	1410		?
AZEL030-18	fixed az, el	Az sweep	1410		?
AZEL015-18	fixed az, el	Az sweep	1410		?

ORCID iDs

G. R. Harp  <https://orcid.org/0000-0002-5060-3470>
 D. G. Messerschmitt  <https://orcid.org/0000-0002-5889-7346>
 Douglas A. Vakoch  <https://orcid.org/0000-0003-3354-9027>

References

- Barott, W. C., Milgrome, O., Wright, M., et al. 2011, *RaSc*, **46**, RS1016
 Boyd, R. W., & Werner, M. W. 1972, *ApJL*, **174**, L137
 Cocconi, G., & Morrison, P. 1959, *Natur*, **184**, 844
 Condon, J. J., Cotton, W. D., Greisen, E. W., et al. 1998, *ApJ*, **115**, 1693
 Cordes, J. M. 2002, in ASP Conf. Ser. 278, Single-Dish Radio Astronomy: Techniques and Applications, ed. S. Stanimirovic et al. (San Francisco, CA: ASP), 227
 Drake, F. D. 1961, *PhT*, **40**, 30
 Drake, F. D. 1965, in Current Aspects of Exobiology, ed. G. Mamikunian & M. H. Briggs (Oxford: Pergamon), 323
 Eaton, J. W., Bateman, D., & Hauberg, S. 1997, Gnu Octave. A High-level Interactive Language for Numerical Computations (Boston, MA: Free Software Foundation)
 Fano, R. M. 1951, Signal-To-Noise Ratio in Correlation Detectors, Tech. Rep. 186 NP-3081 (Cambridge, MA: MIT), <https://dspace.mit.edu/bitstream/handle/1721.1/4871/RLE-TR-186-14255009.pdf?sequence=1>
 Gardner, W. A., & Spooner, C. M. 1992, *ITCom*, **40**, 149
 Harp, G. R., Ackermann, R. F., Blair, S. K., et al. 2010a, in Communication with Extraterrestrial Intelligence, ed. D. A. Vakoch (New York: SUNY Press), 45
 Harp, G. R., Ackermann, R. F., Nadler, Z. J., et al. 2011, *ITAP*, **59**, 2004
 Harp, G. R., Ackermann, R. F., Olsen, E., & Bhatt, A. 2010b, SetiQuest Wiki, http://wiki.setiquest.info/index.php/SetiQuest_Data_Links
 Harp, G. R. R., Richards, J., Shostak, S., et al. 2015, *ApJ*, **825**, 155
 Jones, H. W. 1995, in ASP Conf. Ser. 74, Progress in the Search for Extraterrestrial Life, ed. G. S. Shostak (San Francisco, CA: ASP), 369
 Korpela, B. E., Werthimer, D., Anderson, D., Cobb, J., & Lebofsky, M. 2001, *CSE*, **3**, 78
 Leeb, W. R., Alves, J., Meingast, S., & Brunner, M. 2015, *A&A*, **574**, A9
 Leshem, A., van der Veen, A., Boonstra, A., van der Veen, J., & Boonstra, A. 2000, *ApJS*, **131**, 355
 McQuillan, A., Mazeh, T., & Aigrain, S. 2014, *ApJS*, **211**, 24
 Messerschmitt, D. G. 2012, *AcAau*, **81**, 227
 Messerschmitt, D. G., & Morrison, I. S. 2012, *AcAau*, **78**, 80
 Morrison, I. S. 2011, ATA Memo Ser., 93, 1, <https://www.seti.org/ata-memo-series>
 Morrison, I. S. 2012, *AcAau*, **78**, 90
 Morrison, I. S. 2017, PhD thesis, Univ. New South Wales, <http://handle.unsw.edu.au/1959.4/58502>
 Oliver, B. M., & Billingham, J. 1971, Project Cyclops: A Design Study of a System for Detecting Extraterrestrial Intelligent Life., The 1971 NASA/ASEE Summer Fac. Fellowship Program (NASA-CR-114445), Vol. 1 (Palo Alto, CA: NASA), http://ntrs.nasa.gov/archive/nasa/casi.ntrs.nasa.gov/19730010095_1973010095.pdf
 Rickett, B. J., Kedziora-Chudczer, L., & Jauncey, D. L. 2002, *ApJ*, **581**, 103R
 Shostak, G. S. 1995, in ASP Conf. Ser. 74, Progress in the Search for Extraterrestrial Life, ed. G. S. Shostak (San Francisco, CA: ASP), 447
 Shuch, H. P. 2011, Searching for Extraterrestrial Intelligence: SETI Past, Present, and Future (Berlin: Springer)
 Siemion, A., Von Korff, J., McMahon, P., et al. 2010, *AcAau*, **67**, 1342
 Tarter, J. C. 2001, *ARA&A*, **39**, 511
 Tarter, J. C., Agrawal, A., Ackermann, R., et al. 2010, *Proc. SPIE*, **7819**, 781902
 Von Korff, J., Demorest, P., Heien, E., et al. 2013, *ApJ*, **767**, 40
 Wayth, R. B., Briskin, W. F., Deller, A. T., et al. 2011, *ApJ*, **735**, 97
 Weisberg, J. M., Johnston, S., Koribalski, B., & Stanimirovic, S. 2005, *Sci*, **309**, 106
 Welch, J., Backer, D., Blitz, L., et al. 2009, *IEEEP*, **97**, 1438
 Wozencraft, J. M., & Jacobs, I. M. 1990, Principles of Communication Engineering (Prospect Heights, IL: Waveland)
 Zackay, B., & Ofek, E. O. 2017, *ApJ*, **835**, 11